SUPPLEMENTARY INFORMATION

Source Apportionment of $PM_{2.5}$ in Montréal, Canada and Health Risk Assessment for Potentially Toxic Elements

Nansi Fakhri [a,b], Robin Stevens [b], Arnold Downey [b], Konstantina Oikonomou [c], Jean Sciare [c], Charbel Afif* [a,c], Patrick L. Hayes* [b]

[a] EMMA Research Group, Centre d'Analyses et de Recherche, Faculty of Sciences, Université Saint-Joseph, Beirut, Lebanon

[b] Department of Chemistry, Faculty of Arts and Sciences, Université de Montréal, Montréal, Québec, Canada

[c] Climate and Atmosphere Research Center (CARE-C), The Cyprus Institute, Nicosia, Cyprus

Table S1: Values of the cancer slope factor (CSF) and inhalation unit risk (IUR).

	Cancer slope factor (CSF) (kg·day/mg)			**Inhalation unit risk (IUR) (m^3/mg)**
	Dermal	**Ingestion**	**Inhalation**	
Co			9.8	9
Cr(VI)	20	0.5	41	84
Ni			0.84	0.26
V				8.3
Cd			6.3	1.8
Pb	0.0085	0.0085	0.042	0.000012

Table S2: Displacement error estimation and mapping of bootstrap factors to constrained factors for the PMF model.

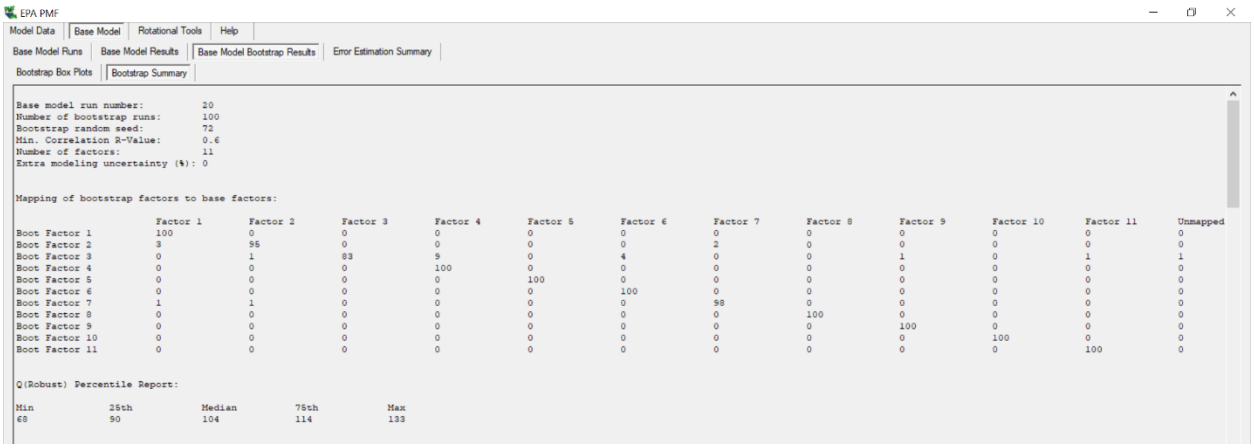

In order to reduce the range of the meaningful number of factors, two parameters was calculated: the maximum individual mean (IM) and the maximum individual standard deviation (IS) where (Lee et al., 1999):

$$IM = \max_{j=1\ldots m}\left(\frac{1}{n}\sum_{i=1}^{n} r_{ij}\right) \quad \text{and} \quad IS = \max_{j=1\ldots m}\left(\sqrt{\frac{1}{n-1}\sum_{i=1}^{n}(r_{ij} - \bar{r}_j)^2}\right)$$

$$r_{ij} = \frac{e_{ij}}{s_{ij}}$$

When the number of factors increases to a critical value, IM and IS will show a drastic drop.

Graphical representations of the IM and IS (**Fig. S6- 1**) revealed a steady drop in their values as the number of factors increased and a stabilization starting with the 11-factor solution. Moreover, a 12-factor solution resolved a phantom factor that could not be definitively linked to a particular source, while a 10-factor solution consolidated two sources into a single factor.

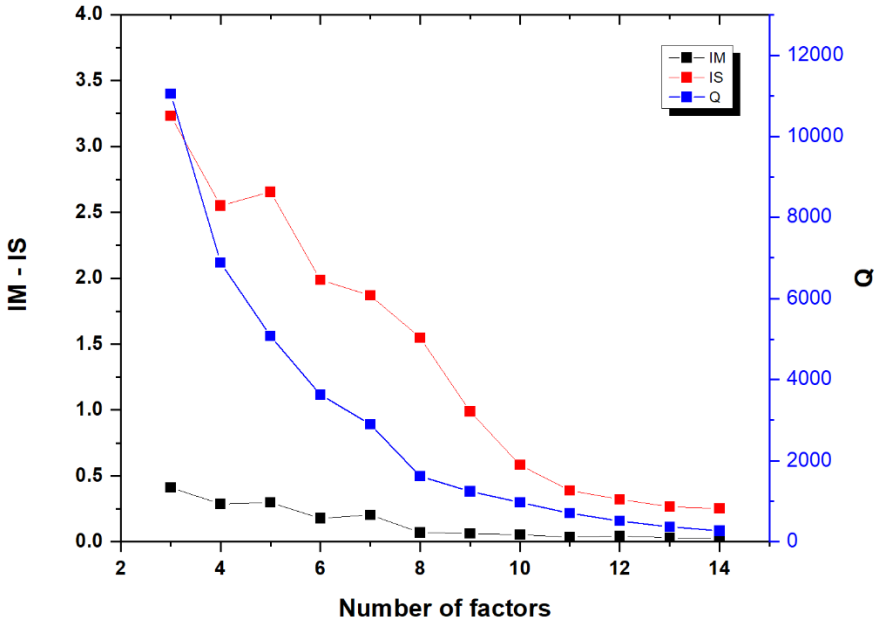

Fig. S1: IM, IS and Q-values for Hersh and USJ sites.

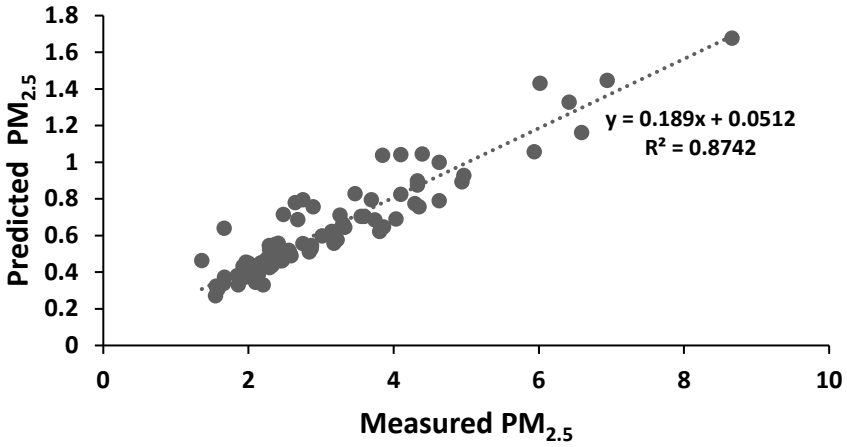

Fig. S2: Measured versus predicted $PM_{2.5}$ concentrations.

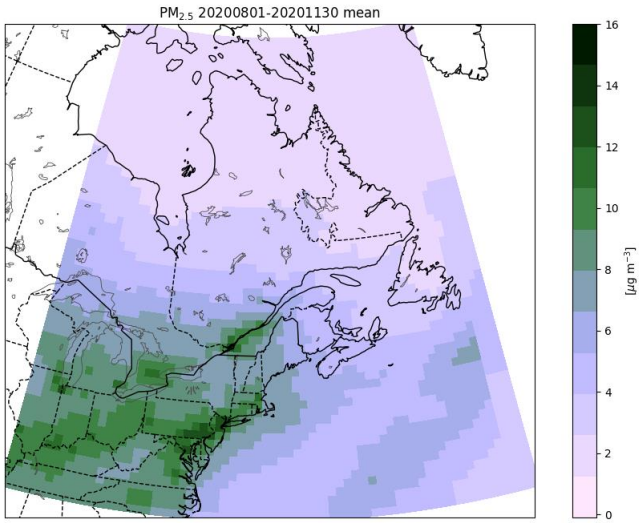

Fig. S3: Mean concentrations of $PM_{2.5}$ from the base case 0.5x0.625 nested GEOS-Chem simulation.

Evaluation of GEOS-Chem against measurements

The model performance was evaluated for $PM_{2.5}$, SO_4^{2-}, NO_3^-, NH_4^+, OC and EC and the results are summarized in **Table S3**. The metrics used for the evaluation were: Pearson's correlation coefficient (R), mean error (ME), normalized mean error (NME), mean bias (MB), and normalized mean bias (NMB). ME, NME, MB, and NMB are calculated following the Eqs. 1-4, where x_i indicates the model predictions and y_i indicates the observed data for a given month and station, both as daily averages, and N is the number of model-observation pairs:

$$\mathrm{ME} = \frac{1}{N}\sum_{i=1}^{N}|x_i - y_i| \qquad \text{(Eq. 1)}$$

$$\mathrm{NME} = \frac{1}{N}\sum_{i=1}^{N}\frac{|x_i - y_i|}{y_i}\cdot 100 \qquad \text{(Eq. 2)}$$

$$\mathrm{MB} = \frac{1}{N}\sum_{i=1}^{N} x_i - y_i \qquad \text{(Eq. 3)}$$

$$\mathrm{NMB} = \frac{1}{N}\sum_{i=1}^{N}\frac{(x_i - y_i)}{y_i}\cdot 100 \qquad \text{(Eq. 4)}$$

Table S3: Evaluation of the GEOS-Chem base case simulation vs measurements from our measurement site.

Pollutants	**R**	**ME**	**NME [%]**	**MB**	**NMB [%]**
$PM_{2.5}$ (μg m^{-3})	0.63	4.69	141.08	4.46	133.98
SO_4^{2-} (μg m^{-3})	0.24	0.43	77.14	0.18	32.39
NO_3^- (μg m^{-3})	0.56	0.30	107.92	0.11	40.95
NH_4^+(μg m^{-3})	0.46	0.23	89.09	0.15	57.08
OC (μg m^{-3})	0.76	0.89	51.46	0.11	41.02
EC (μg m^{-3})	0.57	0.16	58.84	0.01	2.89

We note that significant errors are expected due to the differences in spatial extent of the model resolution (0.5 degrees latitude by 0.625 degrees longitude) versus the observations (essentially a point measurement) as discussed by Schutgens et al. (2016). However, this bias is expected to affect all of the sensitivity simulations in a similar way and would not affect the relative differences between simulations that we use to help interpret the results of the PMF analysis. Furthermore, GEOS-Chem results have been previously used for source contribution analysis similar to the analysis presented in this study (Meng et al. 2019).

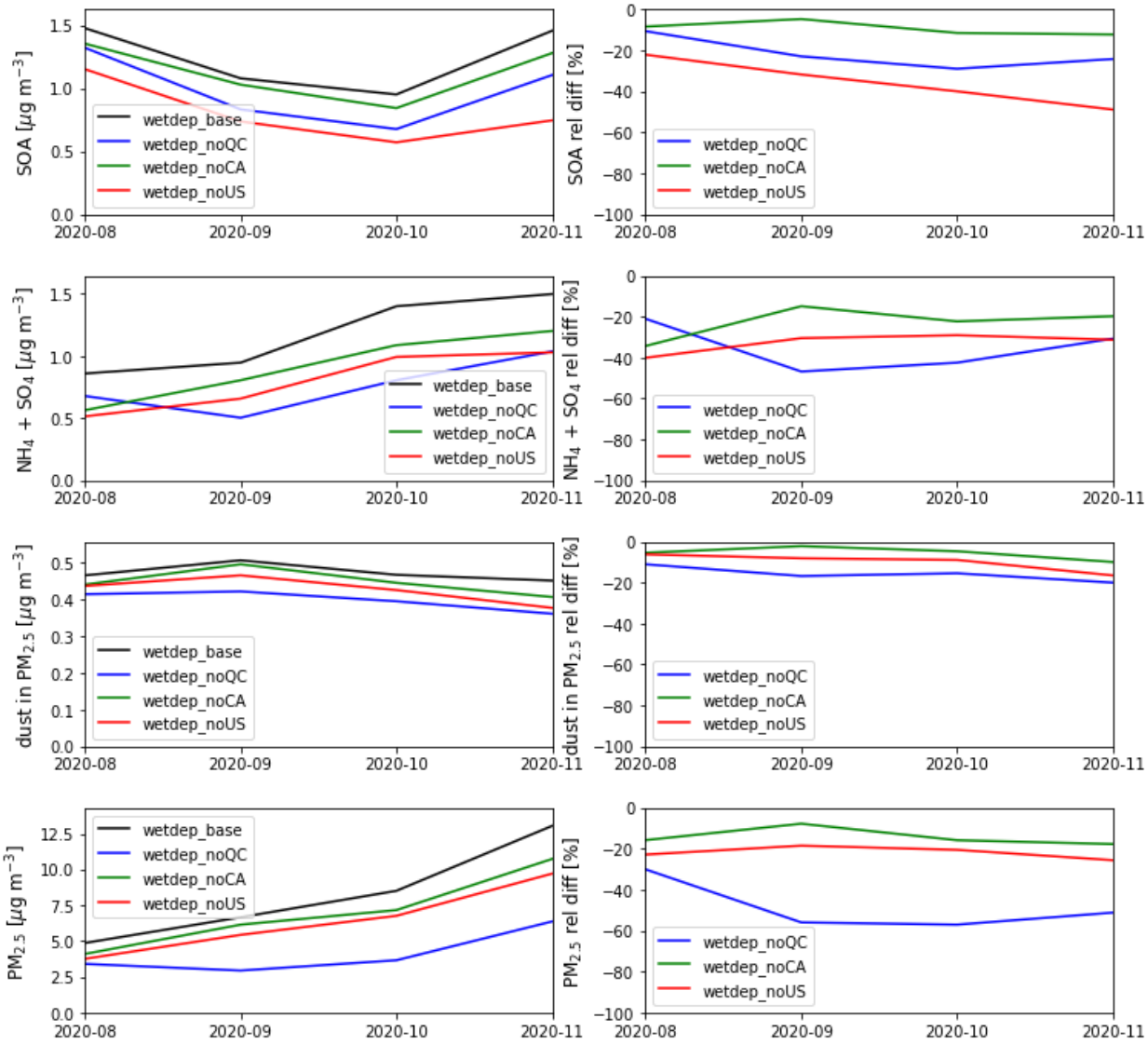

Fig. S4: GEOS-Chem simulations of (top) SOA, (middle 1) the sum of ammonium and sulfate concentrations, (middle 2) dust in $PM_{2.5}$, and (bottom) $PM_{2.5}$. The labels noQC, noCA, and noUS refer to simulations without anthropogenic emissions from Quebec, the rest of Canada, and the US, respectively.

Chemical mass closure

A chemical mass closure study was performed using the chemical composition measurements to estimate the contributions of the different components to the total $PM_{2.5}$ mass concentration following the method reported by Fakhri et al. (2022). Briefly, the contribution of sea salt is calculated by summing the six major ions (Sciare et al., 2005):

$$[\text{Sea salt}] = [Na^+] + [Cl^-] + [ss - Mg^{2+}] + [ss - K^+] + [ss - Ca^{2+}] + [ss - SO_4^{2-}] \quad (Eq.\,5)$$

Ionic constituents such as K^+, Ca^{2+}, Mg^{2+} and SO_4^{2-} are derived from both marine and non-marine sources. Therefore, it is necessary to discriminate sea salt (ss) from non-sea salt (nss) contributions. Assuming that all sodium ions are of marine origin, the sea salt contribution can be calculated based on sea water composition as shown in Eqs. 6 - 9 (Genga et al., 2017; Sciare et al., 2005). Furthermore, non-sea salt potassium, calcium, magnesium and sulfate (nss-K^+, nss-Ca^{2+}, nss-Mg^{2+} and nss-SO_4^{2-}) are calculated by subtracting the sea-salt fraction (ss-K^+, ss-Ca^{2+}, ss-Mg^{2+} and ss-SO_4^{2-}, respectively) from the total concentration of the ions (K^+, Ca^{2+}, Mg^{2+} and SO_4^{2-}, respectively).

$$[ss - SO_4^{2-}] = 0.252 \times [Na^+] \quad (Eq.\,6)$$
$$[ss - Ca^{2+}] = 0.038 \times [Na^+] \quad (Eq.\,7)$$
$$[ss - K^+] = 0.036 \times [Na^+] \quad (Eq.\,8)$$
$$[ss - Mg^{2+}] = 0.119 \times [Na^+] \quad (Eq.\,9)$$

In addition, secondary inorganic aerosol (SIA) is represented by the sum of nss-SO_4^{2-}, NH_4^+ and NO_3^-. To take bound water into account a hydration multiplication factor of 1.29 was applied to convert the dry inorganic concentrations (SIA and sea salt) into hydrated species (Sciare et al., 2005; Genga et al., 2017).

The contribution of crustal matter (CM) (Eq. 10) was estimated by summing the concentrations of aluminum, silicon, calcium, iron, and titanium in their oxide forms (Huang et al., 2014). The coefficients in front of the elements correspond to the additional mass due to oxygen in the minerals. Silicon was not measured in this study and was indirectly determined by multiplying the measured aluminum concentration by a factor of 3.41 (Esmaeilirad et al., 2020). This factor is obtained from the ratio of Si and Al in the Earth's crust following Mason and Moore (1982).

$$[\mathrm{CM}] = 2.2\,[\mathrm{Al}] + 2.49\,[\mathrm{Si}] + 1.63\,[\mathrm{Ca}] + 2.42\,[\mathrm{Fe}] + 1.94\,[\mathrm{Ti}] \qquad (\mathrm{Eq.}\,10)$$

To find the optimal CF to calculate OM from OC, the factor was varied from 1.2 to 2.1. The Pearson correlation (R) calculated between the reconstructed $PM_{2.5}$ and the measured mass did not change significantly (0.978-0.979), but the highest correlation and the slope closest to 1 was obtained with CF=1.6. The results of chemical mass closure study are shown in Fig. S5.

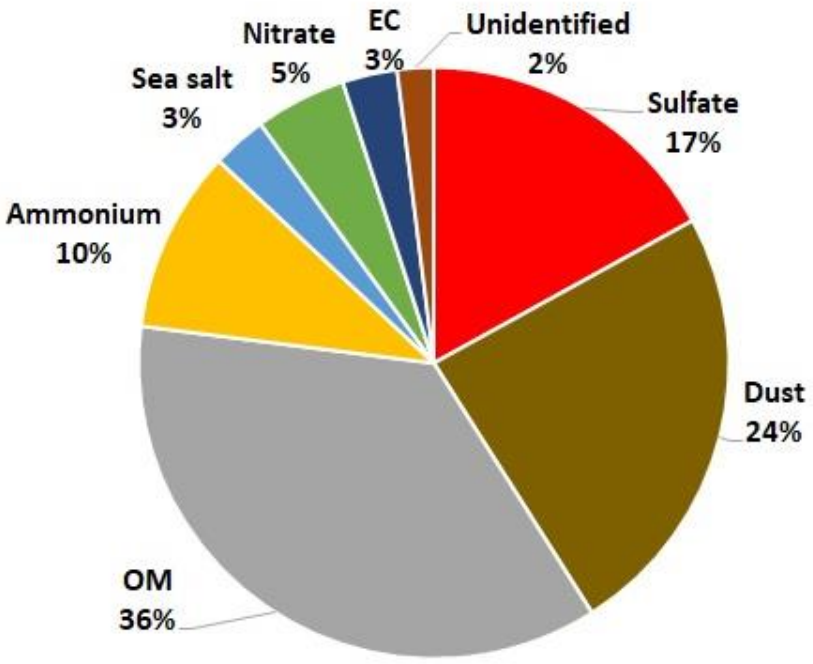

Fig. S5: Percent source contributions determined by chemical mass closure.

The indexes for the n-alkanes

Overall CPI and high CPI were calculated using the concentrations of n-alkanes following the Eq. 11 and 12 (Bray and Evans, 1961; Cooper and Bray, 1963; Fadel et al., 2021):

$$\text{Overall CPI} = \frac{\Sigma \text{ odd C15}-\text{C29}}{\Sigma \text{ even C16}-\text{C30}} \qquad \text{(Eq. 11)}$$

$$\text{High CPI} = \frac{\Sigma \text{ odd C25}-\text{C29}}{\Sigma \text{ even C26}-\text{C30}} \qquad \text{(Eq. 12)}$$

Biogenic sources emit larger amounts of odd carbon number alkanes than even carbon number alkanes, resulting in an Overall CPI greater than 6. Petrogenic emissions, on the other hand, have no carbon preference and have an Overall CPI value close to 1, whereas biomass burning has a value between 2 and 5 (Haque et al., 2019; Li et al., 2010; Fadel et al., 2021). When only the higher

molecular weight n-alkanes are considered, anthropogenic sources have CPI values below 1.5, while biogenic sources have CPI values higher than 3 (Caumo et al., 2020; Kang et al., 2020).

Furthermore, wax n-alkane concentrations were used to assess the relative contributions of biogenic and anthropogenic sources. The concentrations of wax n-alkanes (WNA), in the C14 to C30 range, and its percentage (%WNA) were calculated using the following equations (Fadel et al., 2021):

$$\mathrm{WNA_n} = \mathrm{C_n} - 0.5(\mathrm{C_{n-1}} + \mathrm{C_{n+1}}) \qquad (\mathrm{Eq.}\,13)$$

$$\%\mathrm{WNA} = \frac{\sum \mathrm{WNA}}{\sum \mathrm{NA}} \times 100 \qquad (\mathrm{Eq.}\,14)$$

where C_n is the odd carbon congener, ΣWNA is the sum of wax n-alkane concentrations and ΣNA is the total concentration of n-alkanes. The %WNA value of 7.95±4.93% was indicative of smaller relative inputs from biogenic sources compared to the anthropogenic ones. Hence, the Overall CPI, High CPI and %WNA all appear to depict a similar picture of the anthropogenic origins of n-alkanes.

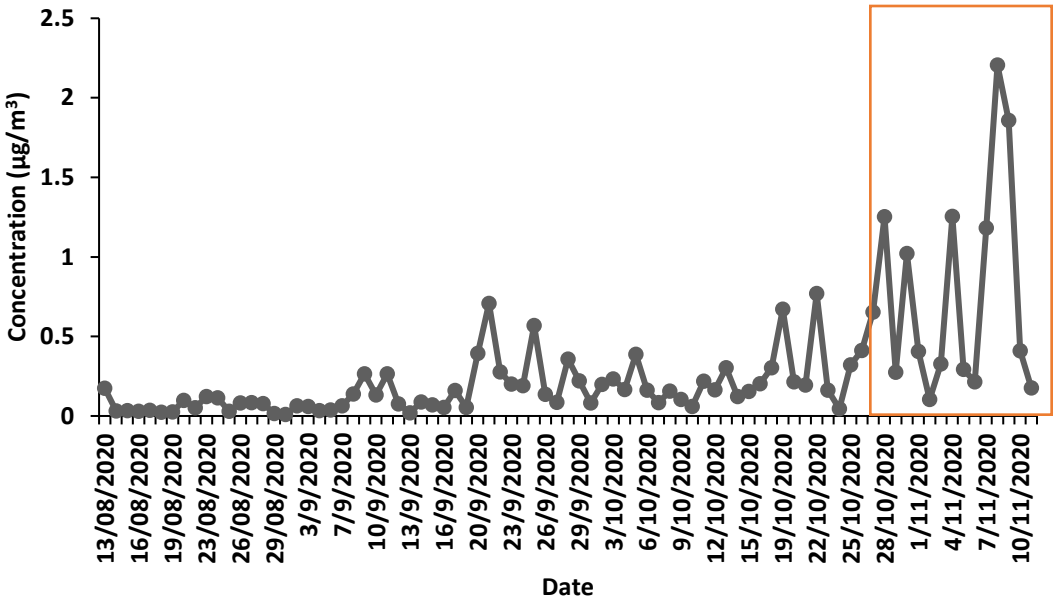

Fig. S6: The temporal variation of nitrate concentrations for the sampling period at MTL site.

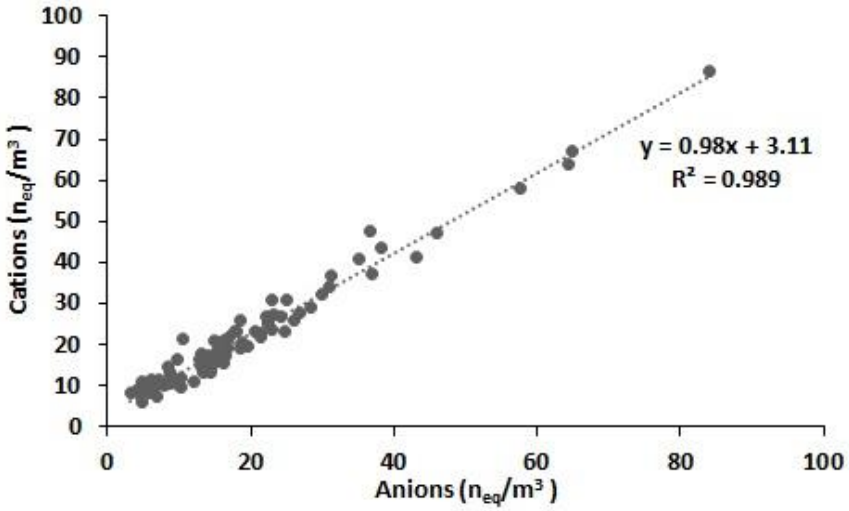

Fig. S7: Ion balance evaluation between the water-soluble ions (Cations: Na^+, Mg^{2+}, NH_4^+, K^+, Ca^{2+} and anions: SO_4^{2-}, NO_3^-, Cl^-).

References

Bray, E.E., Evans, E.D., 1961. Distribution of n-paraffins as a clue to recognition of source beds. Geochim. Cosmochim. Acta 22, 2–15. https://doi.org/10.1016/0016-7037(61)90069-2

Caumo, S., Bruns, R.E., Vasconcellos, P.C., 2020. Variation of the distribution of atmospheric n-alkanes emitted by different fuels' combustion. Atmos. 11, 1–19. https://doi.org/10.3390/atmos11060643

Cooper, J.E., Bray, E.E., 1963. A postulated role of fatty acids in petroleum formation. Geochim Cosmochim. Acta 27, 1113–1127. doi:10. 1016/0016-7037(63)90093-0

Fadel, Marc, Ledoux, F., Farhat, M., Kfoury, A., Courcot, D., Afif, C., 2021. PM2.5 characterization of primary and secondary organic aerosols in two urban-industrial areas in the East Mediterranean. J. Environ. Sci. (China) 101, 98–116. https://doi.org/10.1016/j.jes.2020.07.030

Genga, A., Ielpo, P., Siciliano, T., Siciliano, M., 2017. Carbonaceous particles and aerosol mass closure in PM2.5 collected in a port city. Atmos. Res. 183, 245–254.

Haque, M.M., Kawamura, K., Deshmukh, D.K., Fang, C., Song, W., Mengying, B., Zhang, Y.L., 2019. Characterization of organic aerosols from a Chinese megacity during winter: Predominance of fossil fuel combustion. Atmos. Chem. Phys. 19, 5147–5164. https://doi.org/10.5194/acp-19-5147-2019

Huang, X.H.H., Bian, Q., Ng, W.M., Louie, P.K.K., Yu, J.Z., 2014. Characterization of PM2.5 major components and source investigation in suburban Hong Kong: A one year monitoring study. Aerosol Air Qual. Res. 14, 237–250.

Kang, M., Kim, K., Choi, N., Kim, Y.P., Lee, J.Y., 2020. Recent occurrence of PAHs and n-Alkanes in pm2.5 in Seoul, Korea and characteristics of their sources and toxicity. Int. J. Environ. Res. Public Health 17. https://doi.org/10.3390/ijerph17041397

Lee, E., Chan, C.K., Paatero, P., 1999. Application of positive matrix factorization in source apportionment of particulate pollutants in Hong Kong. Atmos. Environ. 33, 3201–3212. https://doi.org/10.1016/S1352-2310(99)00113-2

Li, W., Peng, Y., Bai, Z., 2010. Distributions and sources of n-alkanes in $PM_{2.5}$ at urban, industrial and coastal sites in Tianjin, China. J. Environ. Sci. 22, 1551–1557. https://doi.org/10.1016/S1001-0742(09)60288-6

Mason, B., Moore, C.B., 1982. Principles of Geochemistry, fourth edition. Wiley.

Meng, J., Martin, R. V., Li, C., van Donkelaar, A., Tzompa-Sosa, Z. A., Yue, X., Xu, J.-W., Weagle, C. L., and Burnett, R. T.: Source Contributions to Ambient Fine Particulate Matter for Canada, Environ. Sci. Technol., 53, 10269–10278, https://doi.org/10.1021/acs.est.9b02461, 2019.

Sciare, J., Oikonomou, K., Cachier, H., Mihalopoulos, N., Andreae, M.O., Maenhaut, W., et al., 2005. Aerosol mass closure and reconstruction of the light scattering coefficient over the Eastern Mediterranean Sea during the MINOS campaign. Atmos. Chem. Phys. Discuss. 5, 2427–2461.

Schutgens, N. A. J., Gryspeerdt, E., Weigum, N., Tsyro, S., Goto, D., Schulz, M., and Stier, P.: Will a perfect model agree with perfect observations? The impact of spatial sampling, Atmos. Chem. Phys., 16, 6335–6353, https://doi.org/10.5194/acp-16-6335-2016, 2016.